THE JOURNAL OF PHYSICAL CHEMISTRY C

Article

pubs.acs.org/JPCC

Exploration of the Electronic Structure of Monoclinic α-$Eu_2(MoO_4)_3$: DFT-Based Study and X-ray Photoelectron Spectroscopy

Ali H. Reshak,*[,†,‡] Z. A. Alahmed,[§] J. Bila,[∥] Victor V. Atuchin,[⊥,#,▽] Bair G. Bazarov,[○,●] Olga D. Chimitova,[○] Maxim S. Molokeev,[◆,¶] Igor P. Prosvirin,[□] and Alexander P. Yelisseyev[■]

[†]New Technologies - Research Centre, University of West Bohemia, Univerzitni 8, 306 14 Pilsen, Czech Republic

[‡]Center of Excellence Geopolymer and Green Technology, School of Material Engineering, University Malaysia Perlis, 01007 Kangar, Perlis, Malaysia

[§]Department of Physics and Astronomy, Collage of Science, King Saud University, Riyadh 11451, Saudi Arabia

[∥]Department of Instrumentation and Control Engineering, Faculty of Mechanical Engineering, CTU in Prague, Technicka 4, 166 07 Prague 6, Czech Republic

[⊥]Laboratory of Optical Materials and Structures, Institute of Semiconductor Physics, SB RAS, Novosibirsk 630090, Russia

[#]Functional Electronics Laboratory, Tomsk State University, Tomsk 634050, Russia

[▽]Laboratory of Semiconductor and Dielectric Materials, Novosibirsk State University, Novosibirsk 630090, Russia

[○]Laboratory of Oxide Systems, Baikal Institute of Nature Management, SB RAS, Ulan-Ude, 670047, Russia

[●]Department of Chemistry, Buryat State University, Ulan-Ude 670000, Russia

[◆]Laboratory of Crystal Physics, Kirensky Institute of Physics, SB RAS, Krasnoyarsk 660036, Russia

[¶]Department of Physics, Far Eastern State Transport University, Khabarovsk 680021, Russia

[□]Boreskov Institute of Catalysis, SB RAS, Novosibirsk 630090, Russia

[■]Laboratory of High Pressure Minerals and Diamond Deposits, Institute of Geology and Mineralogy, SB RAS, Novosibirsk 630090, Russia

Supporting Information

ABSTRACT: The powder α-$Eu_2(MoO_4)_3$ sample was prepared by the solid-state reaction method. The phase purity of the final powder product was verified by X-ray diffraction analysis. The constituent element core levels and valence band are measured by X-ray photoelectron spectroscopy as a function of Ar^+ ion (2.5 keV, 7−8 $\mu A/cm^2$) bombardment time. The formation of Mo^{5+} and Mo^{4+} states at high bombardment times was detected. The Eu−O and Mo−O bonding was considered in comparison with other Eu^{3+}- and Mo^{6+}-containing oxides using binding energy difference parameters. The transparency range obtained for the pure α-$Eu_2(MoO_4)_3$ tablet is λ = 0.41−0.97 μm, as estimated at the transmission level of 5%. The short-wavelength cut edge in α-$Eu_2(MoO_4)_3$ is governed by the direct allowed optical transitions within the band gap of E_g = 3.74 eV (300 K). The band structure of α-$Eu_2(MoO_4)_3$ was calculated by *ab initio* methods and strongly different results were obtained for the spin up/down configurations. The Eu-4f states are located around 2.2 eV and −4.0 eV for spin up (↑) and the structures situated at around 6.5 and 5.5 eV for spin down (↓) configuration. The calculated spin magnetic moments are in excellent relation to the Slater-Pauling rule and within the Eu sphere the magnetic moment of 4f electrons is ∼5.99 μB.

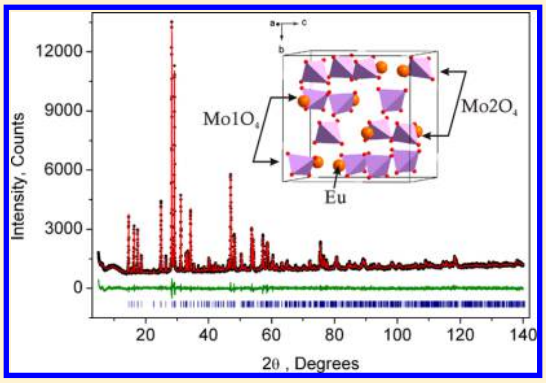

INTRODUCTION

Molybdate crystals are characterized by specific structural characteristics, possess interesting physical and chemical properties, and the materials are widely used in modern catalysis, nanotechnology, electrochemistry, and optics.[1−8] The rare-earth molybdates are of special attention and the materials show a great potential of being used for the preparation of the efficient laser and luminescent media.[9−15] In the phosphor technology, the Eu^{3+} ions doped into the appropriate host matrix provide the efficient red light emission under activation in the UV spectral range.[16−21] However, at special reducing/oxidizing technological conditions, reversible transformation $Eu^{3+}\leftrightarrow Eu^{2+}$ is possible and, respectively, europium in the host matrix can exist in two different formal valence states.[22−24] It is well-known that the spectroscopic

Received: February 12, 2016
Revised: April 19, 2016
Published: April 19, 2016

DOI: 10.1021/acs.jpcc.6b01489
J. Phys. Chem. C 2016, 120, 10559−10568

parameters of Eu^{3+} and Eu^{2+} states are very different and the europium valence state should be precisely controlled to generate phosphor with a predetermined combination of radiative electronic transitions. Thus, the evaluation of the electronic structure of model crystals, where Eu is in the individual formal valence state, is topical.

As it is known, low-temperature monoclinic α-$Eu_2(MoO_4)_3$, space group $C2/c$, is a stable polymorphous modification at room conditions and it can be taken as a representative crystal containing Eu^{3+} ions.[25−27] Thus, in the present study, α-$Eu_2(MoO_4)_3$ molybdate is synthesized and their electronic structure is explored by X-ray photoelectron spectroscopy (XPS) and theoretical methods. It should be pointed that in the α-$Eu_2(MoO_4)_3$ structure the europium ions are in the position with symmetry C_1 and this avoids symmetrical constraints on the electronic parameters of Eu^{3+} ions.

EXPERIMENTAL METHODS

The powder α-$Eu_2(MoO_4)_3$ sample was prepared by the solid state synthesis method. The details of the starting and intermediate reagent preparation and thermal treatment conditions can be found elsewhere.[26] The phase composition of the final powder product was tested by X-ray diffraction (XRD) measurements using an D8 ADVANCE Bruker diffractometer (VANTEC liner detector, CuK_α radiation).[28,29] The XRD pattern from the powder $Eu_2(MoO_4)_3$ sample was recorded at ambient conditions and the earlier reported cell parameters and atom coordinates of the monoclinic phase were taken as a starting model in the structural refinement.[26] The Rietveld refinement was performed using program TOPAS 4.2.[30]

The transmission spectra were recorded at room temperature for a translucent pellet, 150 μm thick, pressed from α-$Eu_2(MoO_4)_3$ powder. The optical measurements were carried out using a UV-2501PC Shimadzu spectrometer over the UV-near-IR spectral region and a Fourier transform spectrometer Infralum FT 801 in the mid-IR. An attempt was made to evaluate the dominant mechanism of electronic band-to-band transitions. As it is known, the transition kind can be obtained from the functional relationship between optical absorption α and photon energy $h\nu$.[31−33] Thus, for direct-allowed and indirect-allowed transitions, relations $\alpha h\nu \propto (h\nu - E_g)^{1/2}$ and $\alpha h\nu \propto (h\nu - E_g)^2$ are obeyed, respectively. The estimations were carried out for a tablet fabricated from a mixture of α-$Eu_2(MoO_4)_2$ and KBr. Band gap values E_g were found by extrapolation of the linear part of $(\alpha h\nu)^2$ versus $h\nu$ or $(\alpha h\nu)^{1/2}$ versus $h\nu$ curves to $\alpha(h\nu) = 0$.

The XPS spectra were measured on a SPECS (Germany) photoelectron spectrometer equipped by a hemispherical PHOIBOS-150-MCD-9 analyzer (Al K_α radiation, $h\nu$ = 1486.6 eV, 200 W). Initially, the binding energy (BE) scale was calibrated in reference to the positions of the peaks of Au $4f_{7/2}$ (BE = 84.0 eV) and Cu $2p_{3/2}$ (BE = 932.67 eV) core levels.[34,35] The sample in the form of powder was deposited onto a conducting double-sided copper scotch. The BE values of the peaks were calibrated in reference to the position of the C 1s peak (BE = 284.8 eV) appeared due to the surface hydrocarbon-like deposits (C−C and C−H bonds). The survey spectrum was recorded at the pass energy of the analyzer being equal to 20 eV. The narrow spectral regions of the valence band, Eu 4d, Mo 3d, C 1s, O 1s, Eu MNN, and Eu 3d levels have been recorded at the pass energy of the analyzer being equal to 10 eV. The surface element concentration ratios were calculated from the photoelectron peak intensities using the theoretical sensitivity factors based on Scofield photoionization cross sections.[36] The ion bombardment of the sample was performed using an argon ion gun (SPECS model IQE 11/35). The energy of Ar^+ ions, the current density and the beam angle were 2.5 keV, 7−8 $\mu A/cm^2$, and 45°, respectively. The depth profiling rate under these conditions was estimated as ∼0.3 nm/min in reference to the Y_2O_3/Si system.[37]

DETAILS OF CALCULATIONS

The electronic and magnetic properties of α-$Eu_2(MoO_4)_3$ compounds were calculated using the all-electron full potential linear augmented plane wave plus the local orbitals (FPLAPW +lo) method accomplished using the WIEN2k code.[38] The experimental structural geometry[26] was optimized using the FPLAPW+lo method[38] within the generalized gradient approximation (PBE-GGA).[39] The optimized atom coordinates used in the calculations can be found in Table S3. For the highly correlated compounds, including oxides, the local density approximation (LDA) and GGA are known to fail to yield the correct ground state. In the systems, the electrons are highly localized. Respectively, the Coulomb repulsion between the electrons in open shells should be accounted. There is no exchange correlation functional, however, that can include this in an orbital independent way, and a simpler approach consists in adding the Hubbard-like on-site repulsion to the Kohn−Sham Hamiltonian. The method is known as LDA+U or GGA+U calculations. There are different ways for the implementation. In the present work, the method of Anisimov et al.[40] and Liechtenstein et al.[41] is applied where the Coulomb (U) and exchange (J) parameters are used.

The ground state properties were determined from the obtained relaxed geometry using FPLAPW+lo[39,42,43] within GGA+U (U - Hubbard Hamiltonian). We applied U on the 4f orbital of Eu atoms and the 4d orbital of Mo atoms. We tested several values for U and it was found that the best U values are 0.55 Ry for the 4f orbital of Eu atoms and 0.22 Ry for the 4d orbital of Mo atoms, which brings the calculated energy band gap in good agreement with the experimental one. We should emphasize that for strongly correlated electron materials the failure of the standard DFT can also be overcome by other approaches that go beyond DFT such as the hybrid functionals (computationally expensive). The hybrid functionals involve the DFT correlation and a mixing of the local or semilocal DFT exchange with the nonlocal Hartree−Fock (HF) exchange in a certain proportion to reduce the self-interaction error of DFT. In fact, it is reported that the hybrid functional, such as HSE06 functional, can be used to describe the bands of nonbonding Ln 4f electrons correctly.[44,45]

The potential for the basis functions construction inside the sphere of the muffin tin was spherically symmetric, whereas it was constant outside the sphere. Self-consistency is reached using 300 $\vec{k}$ points in the irreducible Brillouin zone (IBZ). The self-consistent calculations are converged because the total energy of the system is stable within 0.00001 Ry. The electronic band structure and the related properties were performed within 600 $\vec{k}$ points in the IBZ.

RESULTS AND DISCUSSION

X-ray Diffraction and Optical Measurements. The prepared powder product is of light-cream color common of europium oxides.[21,46,47] The scanning electron microscopy observation indicates the formation of well-faceted partly agglomerated grains with dimensions of 1−15 μm.[26] The phase purity of the α-$Eu_2(MoO_4)_3$ powder sample was confirmed

DOI: 10.1021/acs.jpcc.6b01489
J. Phys. Chem. C 2016, 120, 10559−10568

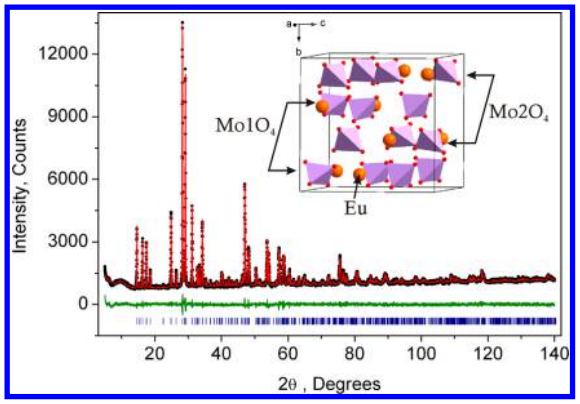

Figure 1. Rietveld difference plot of α-$Eu_2(MoO_4)_3$ at room temperature. The obtained crystal structure of monoclinic α-$Eu_2(MoO_4)_3$ is illustrated in the inset.

by XRD measurements and structural refinement. The measured XRD pattern is shown in Figure 1. The refinement was stable and gave low *R*-factors, and the main structural parameters are given in Table 1. The fractional atomic coordinates and metal−oxygen bond lengths are shown in Tables S1 and S2, respectively. The obtained structural parameters are in good relation to those earlier found for the α-$Eu_2(MoO_4)_3$ phase.[25,26]

Table 1. Main Parameters of Processing and Refinement

compound	α-$Eu_2(MoO_4)_3$
sp. gr.	*C*2/*c*
a, Å	7.5609(1)
b, Å	11.4707(2)
c, Å	11.5122(2)
β, °	109.298(1)
V, Å^3	942.34(3)
Z	4
2θ-interval, °	5−140
no. of reflections	904
no. of refined parameters	69
R_{wp}, %	3.78
R_p, %	2.93
R_{exp}, %	2.97
χ^2	1.28
R_B, %	0.89

The transparency range obtained for the pure α-$Eu_2(MoO_4)_3$ tablet is λ = 0.41−0.97 μm, as estimated at the transmission level of 5% (Figure 2, curve 1). This is an unusually narrow range and, typically, the transparency range in molybdates is noticeably wider. By way of example, the ranges in $Bi_2(MoO_4)_3$, $PbMoO_4$, and $ZnMoO_4$ are as wide as 0.415−5.2, 0.42−3.9, and 0.327−4.96 μm, respectively.[48−51] The comparatively slow transmission increase on the wavelength increase appeared, at least partly, due to light scattering by the powder particles. The sharp absorption lines observed in the visible and ultraviolet parts of the spectrum are related to the 4f−4f transitions in Eu^{3+} ions. Besides, a wide band with its maximum at ~0.40 μm is detected near the short-wavelength cut. This band may be attributed to the absorption of Eu^{3+} ions captured electrons from the nearest point defect. The most intensive absorption lines are attributed to the transitions from $^7F_0$ and $^7F_1$ states to higher energy states $^5D_0$ (590.9 nm), $^5D_1$ (535.7 nm), $^5D_2$ (465.4 nm), $^5D_3$ (420 nm), $^5D_4$ (365.4 nm).[52,53] The noticeable shift of the short-wavelength cut edge to shorter wavelengths in reference to that in other oxides, including molybdates, may be induced by the electron transition into the main multiplet ^7F, when electrons transit from $^7F_0$ to higher energy states ^7F_i, i = 4, 5, 6. The wide short-wavelength absorption bands of Eu^{3+} ions are induced by electron-dipole f−d transitions.[54]

The results of the fundamental absorption edge measurements are shown in Figure 3. The straight-line fitting is performed in coordinates of $(\alpha h\nu)^2 = f(h\nu)$, where α is the absorption coefficient in cm^{-1}, and $h\nu$ is the photon energy in eV. Thus, it is found that, in α-$Eu_2(MoO_4)_3$, the short-wavelength cut edge is governed by the direct allowed optical transitions within the band gap of E_g = 3.74 eV (300 K). The estimated band gap value is among the E_g values earlier observed in other molybdates: 3.2 eV ($PbMoO_4$,[55]), 3.98 eV ($SrMoO_4$,[56]), 4.3 eV ($ZnMoO_4$,[57]). Narrow absorption lines in the 3.4 to 3.85 eV range (Figure 3) observed near the fundamental absorption edge of α-$Eu_2(MoO_4)_3$ are due to 4f−4f electronic transitions in Eu^{3+}. A line near 3.4 eV (365 nm) is related to transition $^7F_0 \rightarrow {}^5D_4$, whereas a group at larger photon energies is associated with transitions $^7F_{1,0} \rightarrow {}^5H_{7,6,5}$.[52,53]

The survey photoelectron spectrum recorded from α-$Eu_2(MoO_4)_3$ powder is shown in Figure S1. All spectral features, except one, were successfully attributed to constituent element Auger lines and core levels. The line at 284.8 eV can be attributed to the C 1s

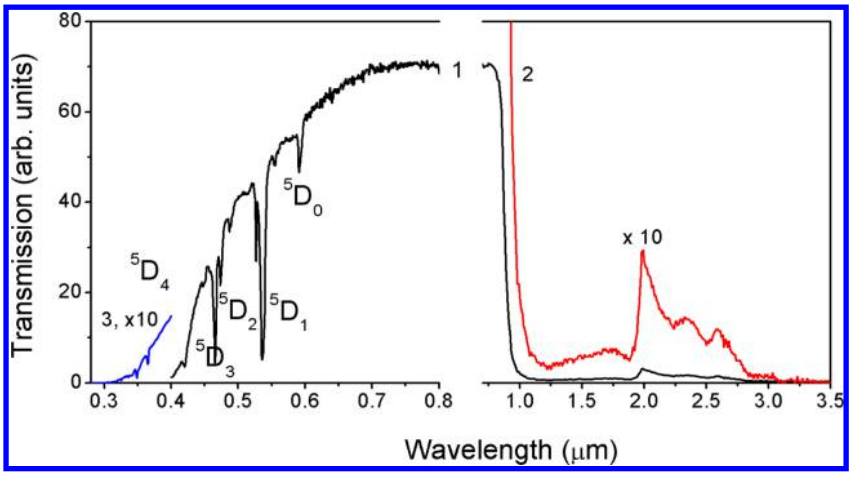

Figure 2. Optical transmission spectra measured for (1) and (2) α-$Eu_2(MoO_4)_3$ tablet, and for (3) mixed α-$Eu_2(MoO_4)_2$ and KBr tablet.

DOI: 10.1021/acs.jpcc.6b01489
J. Phys. Chem. C 2016, 120, 10559−10568

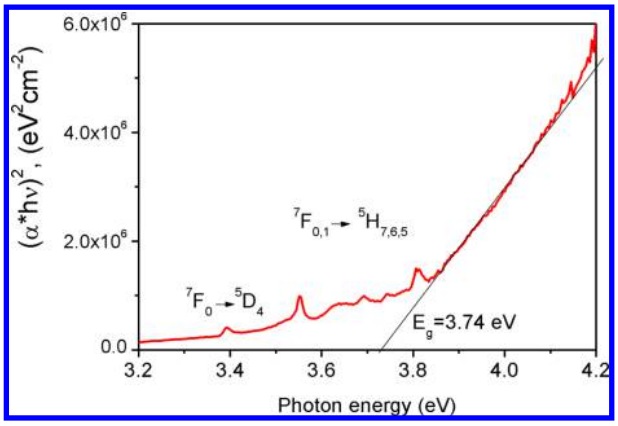

Figure 3. Fundamental absorption edge for the α-$Eu_2(MoO_4)_3$ tablet, as given in coordinates $(\alpha^*h\nu)^2 = f(h\nu)$. T = 300 K.

signal and this line, at least partly, is related to adventitious hydrocarbons adsorbed on the particle surface from the laboratory air. As it is seen from Figure S2, the comparison of the spectra before and after ion bombardment indicates that the C 1s signal can be noticeably decreased by top surface ion sputtering. The α-$Eu_2(MoO_4)_3$ particles are well faceted and, respectively, the adsorbate removal from the flat facets is possible by ion bombardment.

The constituent element core levels are shown in Figures 4–6 and Figure S3. As to the initial surface state, the binding energy

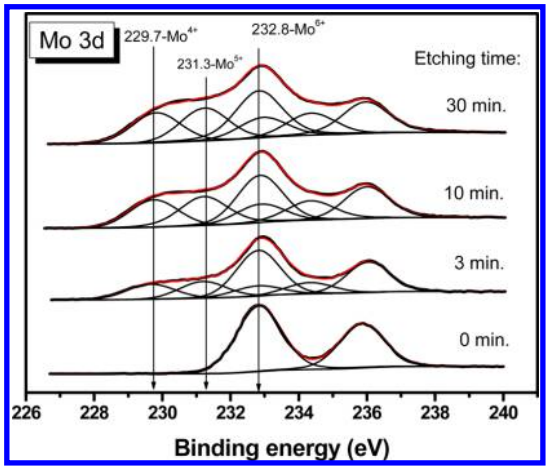

Figure 4. Detailed spectra of the Mo 3d doublet for four selected bombardment times.

values of the representative levels Mo $3d_{5/2}$ and Eu $3d_{5/2}$ fall in the ranges typically observed in Mo^{6+}- and Eu^{3+}-containing oxides.[58−69] Generally, the intensity of the element core levels increases on the bombardment time increase because of contaminated top-surface layer sputtering. As to Mo 3d doublet behavior, however, the appearance of two new components is evident at longer bombardment times and this effect is related to the generation of Mo^{5+} and Mo^{4+} states due to a partial oxygen loss from the surface. It should be emphasized that previously a similar effect of the lower-valence states generation was observed for the W 4f doublet in several tungstate crystals.[70−74] Thus, molybdate and tungstate crystals are unstable under middle-energy Ar^+ ion bombardment, and they possess a general trend of Mo^{6+} and W^{6+} transformation to the lower-valence states in the top-surface layer.

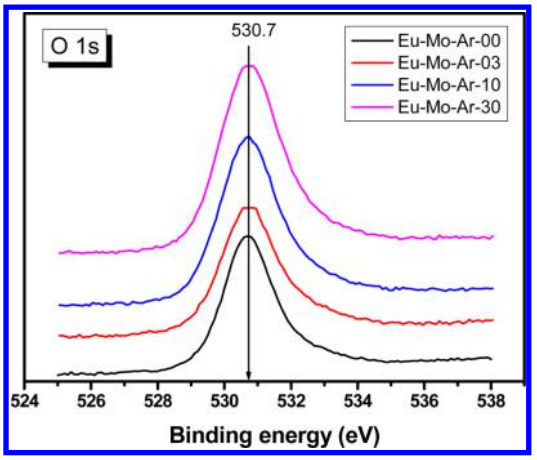

Figure 5. Detailed spectra of the O 1s core level for four selected bombardment times.

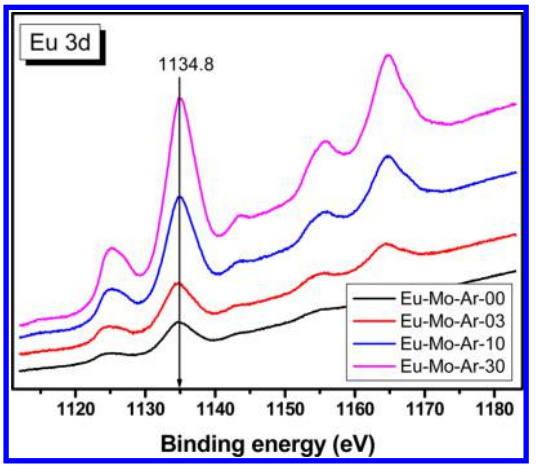

Figure 6. Detailed spectra of the Eu 3d doublet for four selected bombardment times.

In parallel to the Mo^{5+} and Mo^{4+} states formation by ion bombardment, the line of O 1s becomes wider. As it may be supposed, a new component or components appeared in the O 1s band and the components are related to the O^{2+} ions bonding to Mo^{5+} and Mo^{4+} ions.[75] The effect in α-$Eu_2(MoO_4)_3$ powder, however, is not pronounced and the BE(O 1s) value remains to be the same, as it is evident from Figure 5. As to energy positions of the Eu $4d_{5/2}$ and Eu $3d_{5/2}$ lines, these are the effects insensitive to bombardment. Earlier, several other oxide compounds containing Eu^{3+} ions were measured by XPS and noticeably different BE(Eu $4d_{5/2}$) and BE(Eu $3d_{5/2}$) values were obtained in different compounds for the characteristic europium peaks. The experimental data found in the literature for the crystals, where trivalent europium is a constituent element, are shown in Table 2. Here, if the component decomposition was used for the O 1s band, the lower BE component was selected as a representative one of the compound bulk. The drastic scattering of the measured values of BE(Eu $4d_{5/2}$) and BE(Eu $3d_{5/2}$) is evident and this is well illustrated by the parameters reported for the elementary oxide Eu_2O_3 which was measured by XPS several times in the past. Among the strongest factors generating the scattering, the pronounced surface reactivity of many Eu^{3+}-oxide compounds and surface charging effects during XPS measurements could be considered. As it was repeatedly demonstrated in several previous observations, the surface charging effects can be excluded

DOI: 10.1021/acs.jpcc.6b01489
J. Phys. Chem. C 2016, 120, 10559−10568

Table 2. Binding Energy Values in Eu^{3+}-Containing Oxides

crystal	Eu $4d_{5/2}$ (eV)	O 1s (eV)	Eu $3d_{5/2}$(eV)	Δ_{4d}(eV)	Δ_{3d} (eV)	reference
Eu_2O_3	135.0		1134.0 (fixed)			65
	136.5	529.2	1134.6	392.7	−605.4	66
	134.9	529.0	1133.7	394.1	−604.7	67
			~1132			68
		529.2	1133.5		−604.3	69
	135.9	531.1	1135.4	395.2	−604.3	78
$EuNbO_4$	135.8		1134.8			64
$Eu(OH)_3$		528.9	1133.5		−604.6	69
$Eu_2(C_2O_4)_3$	134.4	531.2	1133.9	396.8	−602.7	67
$Eu_2(C_2O_4)_3{\cdot}10H_2O$		531.9	1134.9		−603.0	77
$Eu_2(CO_3)_3$	136.5	531.7	1135.3	395.2	−603.6	67
$Eu_2(SO_4)_3$	136.9	531.9	1135.9	395.0	−604.0	67
$Eu_2(NO_3)_3$	137.7	533.5	1136.4	395.8	−602.9	67
$EuMnO_3$	134.3					76
$EuAlO_3$	135.6	529.6	1133.0	394.0	−603.4	79
$Eu_2(MoO_4)_3$	136.3	530.7	1134.8	394.4	−604.1	Present study

from the consideration if the BE difference is used as a representative parameter instead of the conventional BE value.[61,63,72−74,80−83] Thus, BE difference parameters Δ_{4d} = BE(O 1s − Eu $4d_{5/2}$) and Δ_{3d} = BE(O 1s − Eu $3d_{5/2}$) were also calculated for europium core levels and they are shown in Table 2. Usually, the scattering of the BE difference parameters is lower than that of BE parameters.[80,84] For the Eu-containing crystals listed in Table 2, this, however, is not right. The scattering ranges of BE(Eu $4d_{5/2}$) and BE(Eu $3d_{5/2}$) are 1.5 and 1.9 eV, respectively. Comparatively, the scattering ranges of Δ_{4d} and Δ_{3d} are 2.5 and 1.1 eV. The scattering of Δ_{4d} is even higher than that of BE(Eu $4d_{5/2}$). Thus, it can be concluded that for the crystal set measured by XPS up to the present, the surface reactivity is the main factor governing the experimental data scattering. Among the compounds shown in Table 2, from the chemical point of view, $EuAlO_3$ and $Eu_2(MoO_4)_3$ seem to be the most stable in reference to surface reactivity in the air environment. Other compounds are very hygroscopic or incompletely characterized in literature. For this reason, ranges Δ_{4d} = 394.0−394.4 and Δ_{3d} = −(603.4−604.1) eV could be considered as representative for the characterization of Eu^{3+} states in oxides. However, further accumulation of XPS parameters of different Eu^{3+}-containing crystals is evidently topical.

As to Mo−O chemical bonding effects, these were previously considered in ref 60., where the diagram related to the $\Delta Mo_{3d5/2}$ = BE(O 1s − Mo $3d_{5/2}$) and mean bond length L(Mo−O) was depicted. The coordination of Mo^{6+} ions in α-$Eu_2(MoO_4)_3$ may be considered as tetrahedral and, then, value L(Mo−O) = 180.3 pm can be calculated.[25,26] From the XPS measurements carried out in the present study, we have $\Delta Mo_{3d5/2}$ = 297.9 eV. Thus, in the diagram created in ref 64., the point related to α-$Eu_2(MoO_4)_3$ appears in the cluster of molybdate crystals with tetrahedral coordination of Mo^{6+} ions.

The valence band in α-$Eu_2(MoO_4)_3$ is shown in Figure 7, as measured by XPS for several bombardment times. For the initial surface state, there are two shallow bands with maxima at ~1.7 and ~8 eV. Then, on the bombardment time increase, the intensity of both of these bands also increase. It should be pointed that the intensity of the band at ~1.7 eV grows faster than that of the band at ~8 eV. Besides, the shoulder appears at ~5 eV. As it seems, the effects may be attributed to the generation of the Mo^{5+} and Mo^{4+} states at the top surface of the particles bombarded by Ar^+ ions.

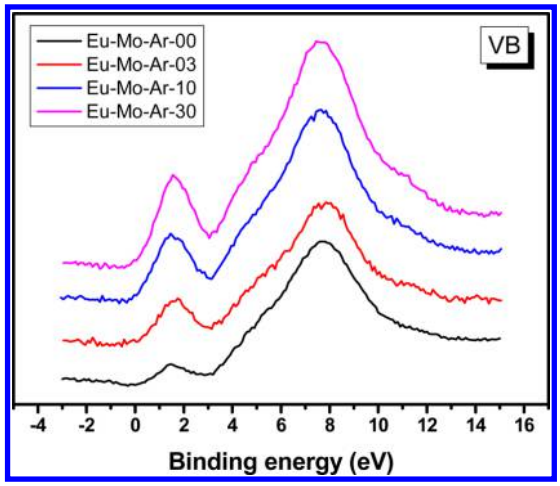

Figure 7. Detailed spectra of the valence band for four selected bombardment times.

Spin Polarized Electronic Band Structure and Density of States. The spin up (↑) and spin down (↓) electronic band structures of the α-$Eu_2(MoO_4)_3$ compound exhibit that this crystal is an indirect band gap semiconductor, as shown in Figure 8a,b. For spin up (↑) and spin down (↓), the valence band maximum (VBM) is located at the Y_0 symmetry point of the first BZ. Whereas the conduction band minimum (CBM) for spin up (↑) is situated at the M_0 point, it is at the Γ point for spin down (↓). The calculated band gaps are 2.2 eV (↑) and 3.2 eV (↓). In this calculation the zero of the energy scale is taken at the top of the valence band. It was noticed that the energy gap of spin up (↑) is noticeably lower than that of spin down (↓). That is attributed to the location of Eu-f at around 2.2 eV for the spin up (↑) that pushes the CBM toward the Fermi level resulting in the reduced energy gap value. Whereas for spin down (↓), the Eu-f states are shifted toward higher energies to be situated around 6.5 eV resulting in a shift of the CBM by around 1.0 eV toward higher energies and that increases the band gap value of spin down (↓) which shows good agreement with the measured one (see Figure 5S). It is interesting to highlight that the CBM for spin up is formed by

DOI: 10.1021/acs.jpcc.6b01489
J. Phys. Chem. C 2016, 120, 10559−10568

the Eu-4f states, while for spin-down it is originated from the Mo-d states revealing that the Eu-4f band vanished. The VBM is formed by O-p states for both spin-up/down configurations. We would like to mention that the Eu states play a role in reducing the band gap in comparison with molybdates where the trivalent cation is not a lanthanide. The same phenomenon has been found to occur in tungstates like $EuWO_4$.[85]

The necessary ingredients of the total and atom-resolved density of states are calculated for the spin up (↑) and spin down (↓) cases, as shown in Figure 8a,b. The total density of states for the spin up (↑) exhibits similar features to that of spin down (↓) except for the location of the Eu-4f band. It is located around 2.2 eV and −4.0 eV for spin up (↑), whereas for the spin down (↓) configuration, both structures which were appeared at 2.2 eV and −4.0 eV in the case of spin up (↑) are shifted toward higher energies to be situated at around 6.5 and 5.5 eV. It is interesting to mention that the appearance of Eu-4f at around 2.2 eV in the spin up configuration is attributed to the charge transfer (CT) from O 2p states to unoccupied spin up Eu 4f states. It is clear that the appearance of Eu-4f at around 2.2 eV in the spin up causes a band gap reduction in concordance with our observation of the electronic band structure. There are two types of charge transfer (CT) in α-$Eu_2(MoO_4)_3$ compounds: the first one is O^{2-}−Mo^{6+} and the second one is O^{2-}−Eu.[86] The calculated values are 3.2 and 2.2 eV, respectively.

We should emphasize that the spin up Eu^{3+} 4f states are split into occupied and unoccupied bands. The occupied spin up Eu^{3+} 4f band is located at −4.0 eV and the unoccupied spin up Eu^{3+} 4f band is located at 2.2 eV. The unoccupied spin down Eu^{3+} 4f states form two bands located at 5.5 and 6.5 eV. Also, by the change of the oxidation state of Eu (from 3+ to 2+), the decreased atomic charge from 3 to 2 leads to a destabilization of the 4f electrons (due to lower Coulomb attraction of 4f electrons in the less positively charged Eu^{2+} cation in comparison with the Eu^{3+} cation) and a uniform shift of the 4f bands by about 5 eV occurs. This shift in Eu^{2+} causes the band of occupied spin up 4f states to be located directly in the gap.[45] Moreover, the presence of unpaired Eu^{3+} 4f electrons causes the spin up and spin down states of Eu^{3+} to be split and the spin up states are shifted down in contrast to the states of Mo^{6+} and O^{2-} (paired electrons), which form compact nonspin separated bands (Figures 8 and 9).

The angular momentum character of various structures in α-$Eu_2(MoO_4)_3$ compounds for the spin up (↑) and spin down

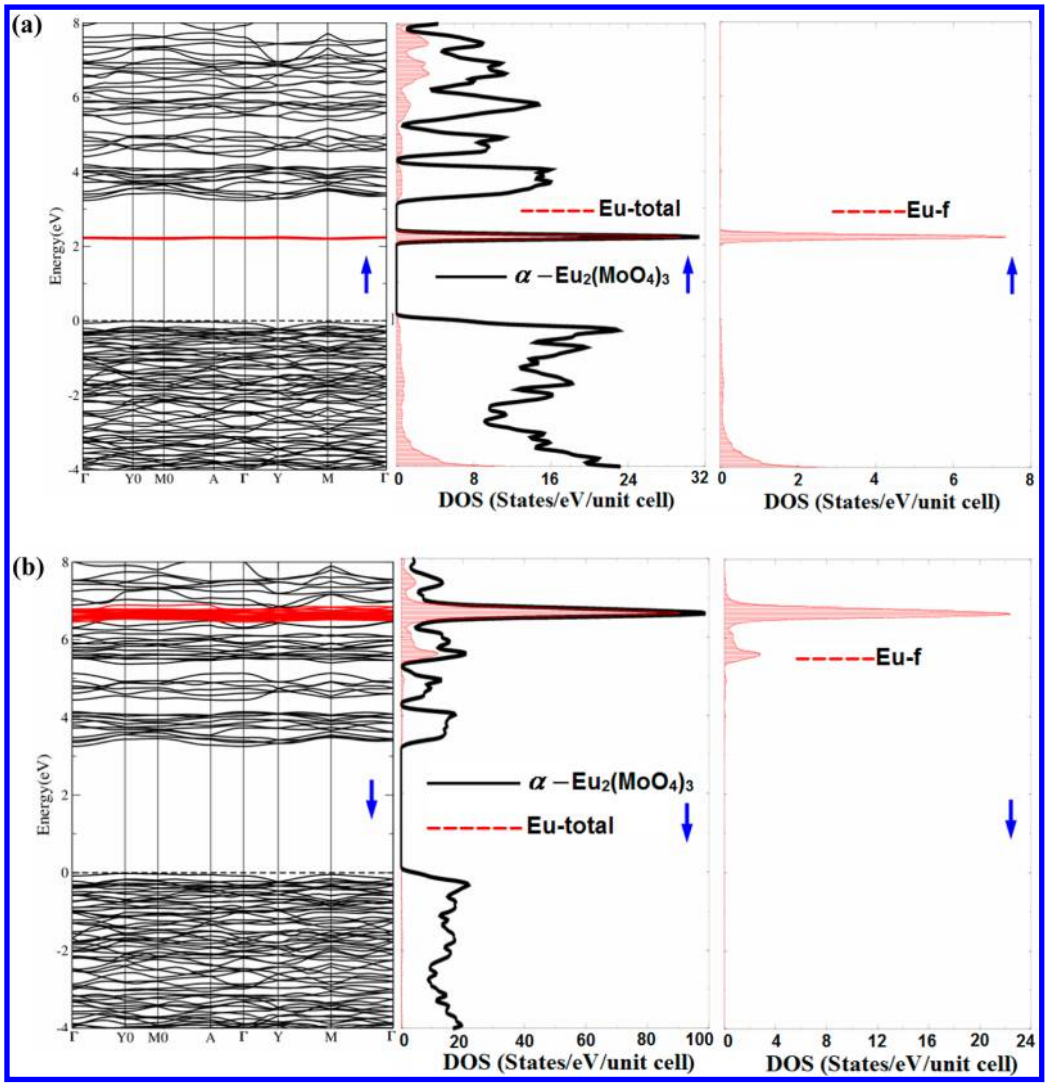

Figure 8. Calculated spin polarized electronic band structure along with the calculated total density of states, density of state of the Eu atom, and Eu-f states for (a) spin up and (b) spin down cases.

DOI: 10.1021/acs.jpcc.6b01489
J. Phys. Chem. C 2016, 120, 10559−10568

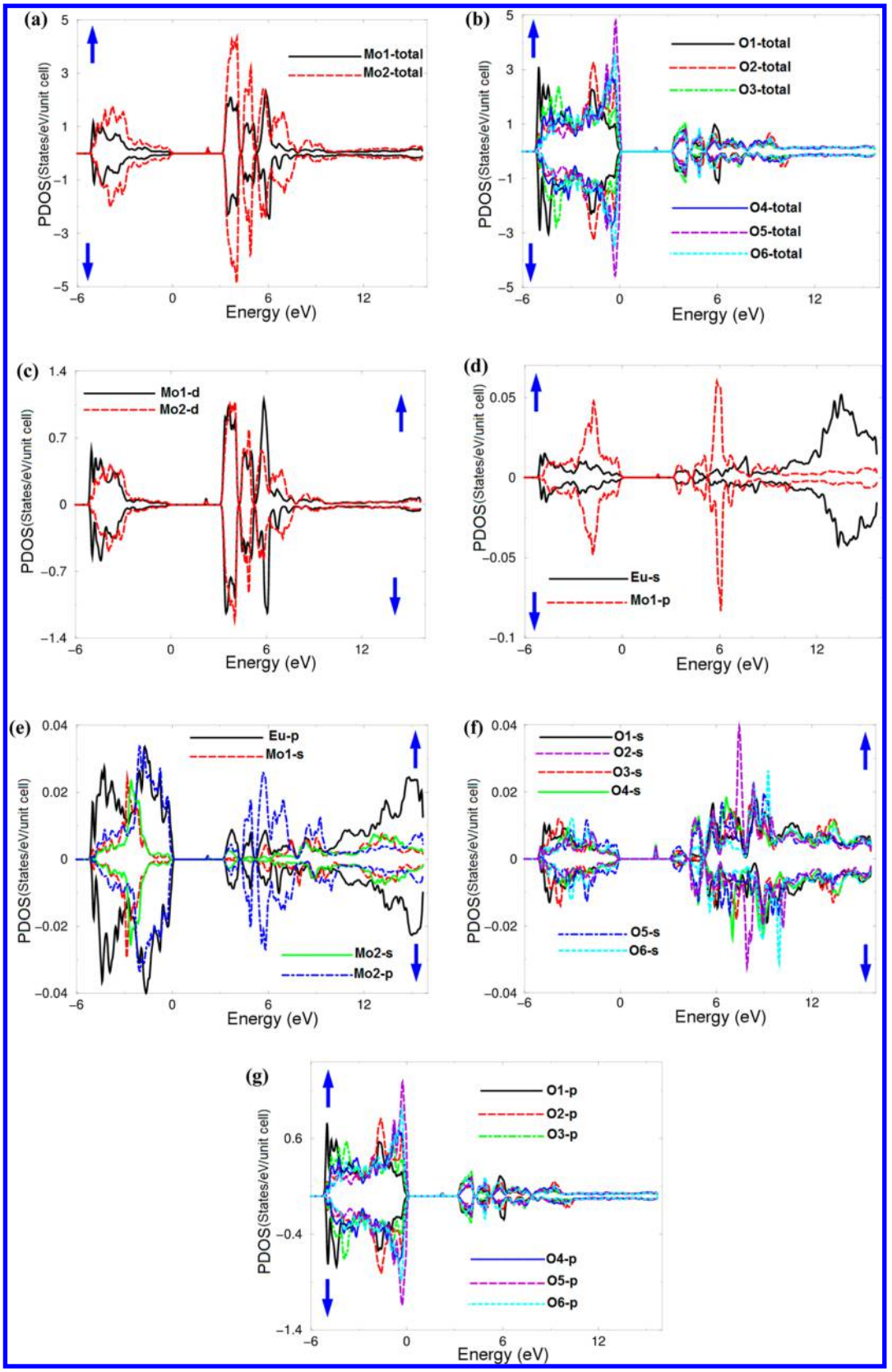

Figure 9. Calculated angular momentum projected density of states (PDOS) for spin up/down configurations. Here, the (a) Mo-total, (b) O-total, (c) Mo-d, (d) Eu-s and Mo1-p, (e) Eu-p, Mo-s, and Mo2-p, (f) O-s, and (g) O-p states are shown.

(↓) states can be obtained by calculation of the angular momentum projected density of states (PDOS), as shown in Figure 9a–g. It was found that the two Mo and six O atoms exhibit significant contributions along the energy scale for spin-up/down (see Figure 9a,b). The Mo-d state is distributed in the valence and conduction bands and shows the main contribution

DOI: 10.1021/acs.jpcc.6b01489
J. Phys. Chem. C 2016, 120, 10559–10568

Table 3. Calculated Atom-Resolved Spin Magnetic Moment (in μB)

Eu (μB)	Mo (μB)	Mo (μB)	O1 (μB)	O2 (μB)	O3 (μB)	O4 (μB)	O5 (μB)	O6 (μB)	interst. (μB)
5.9979	0.00113	−0.00009	−0.00577	−0.01259	−0.00719	−0.01270	−0.00861	−0.00661	0.22415

above the CBM for spin up and at the CBM for spin-down Figure 9c. In Figure 9d−f, we can see that the Eu-s/p, Mo-s/p, and O-s states show a small contribution along the whole energy scale, while O-p states (Figure 9g) exhibit the main contribution below E_F. The spin magnetic moments are calculated for the atom resolved within the muffin-tin spheres, as well as in the interstitial sites, as shown in Table 3. The calculated spin magnetic moments are in accordance with the Slater-Pauling rule. The calculation shows that the magnetic moment of 4f electrons within the Eu sphere is about 5.99 μB. There exists a strong hybridization between Eu-d and Mo-p states below E_F and the O-s state hybridized with Eu-s and Mo-p states above and below E_F. The hybridization degree favors enhancing the covalent bonding.

CONCLUSIONS

In the present work, the electronic structure of α-$Eu_2(MoO_4)_3$ has been explored in detail. For the experimental observation, the high-quality low-temperature modification α-$Eu_2(MoO_4)_3$ has been synthesized in the powder form by the solid state synthesis method. The electronic structure of the α-$Eu_2(MoO_4)_3$ molybdate has been studied by X-ray photoelectron spectroscopy (XPS) and theoretical methods for the first time. The chemical bond analysis has been carried out in comparison of α-$Eu_2(MoO_4)_3$ with many other molybdates and Eu^{3+}-containing compounds using the BE difference parameters. As a result, the BE difference ranges of Δ_{4d} = BE (O 1s − Eu $4d_{5/2}$) = 394.0−394.4 and Δ_{3d} = BE (O 1s − Eu $3d_{5/2}$) = −(603.4−604.1) eV could be considered as representative for the characterization of Eu^{3+} states in oxides. Thus, XPS can be helpful for the europium valence state control in Eu-doped oxides, including phosphors where the europium content is comparatively low.

As is well-known, the band structure of Ln-bearing oxides is very dependent on the energy position of the Ln 4f orbitals in the valence band, and this feature in α-$Eu_2(MoO_4)_3$ is observed in the present study. The family of molybdates $Ln(MoO_4)_3$ is very wide and, respectively, it can be selected as a suitable grounding for the exploration of related electronic and spectroscopic effects generated due to rare-earth (Ln) element substitution and polymorphous phase transitions.

ASSOCIATED CONTENT

Supporting Information

The Supporting Information is available free of charge on the ACS Publications website at DOI: 10.1021/acs.jpcc.6b01489.

Fractional atomic coordinates and the main bond lengths of α-$Eu_2(MoO_4)_3$. Survey photoelectron spectra, detailed spectra of the C 1s line, Eu 4d doublet, and Eu MNN Auger lines for four selected bombardment times. (PDF)

AUTHOR INFORMATION

Corresponding Author

*E-mail: maalidph@yahoo.co.uk. Phone: +420 777729583.

Author Contributions

The manuscript was written through contributions of all authors. All authors have given approval to the final version of the manuscript. All authors contributed equally.

Funding

This work was partly supported by the Russian Foundation for Basic Research (Grants 15-32-50586 and 15-52-53080). V.V.A. gratefully acknowledges the Ministry of Education and Science of the Russian Federation for the financial support. A.H.R. would like to acknowledge the CENTEM project, reg. no. CZ.1.05/2.1.00/03.0088, cofunded by the ERDF as part of the Ministry of Education, Youth and Sports OP RDI program and, in the follow-up sustainability stage, supported through CENTEM PLUS (LO1402) by financial means from the Ministry of Education, Youth and Sports under the "National Sustainability Programme I". Computational resources were provided by MetaCentrum (LM2010005) and CERIT-SC (CZ.1.05/3.2.00/08.0144) infrastructures.

Notes

The authors declare no competing financial interest.

REFERENCES

(1) Schröder, F. A. Contributions to the Chemistry of Mo and W. XIV. The Mo-O Bond Length/Bond Order Relationship. A Systematic Treatment. *Acta Crystallogr., Sect. B: Struct. Crystallogr. Cryst. Chem.* **1975**, *31*, 2294−2309.

(2) Efremov, V. A. Characteristic Features of the Crystal Chemistry of Lanthanide Molybdates and Tungstates. *Russ. Chem. Rev.* **1990**, *59*, 627−642.

(3) Ponomarev, B. K. Magneto-Electrical Properties of Rare Earth Molybdates. *Ferroelectrics* **2002**, *280*, 261−283.

(4) Isupov, V. A. Binary Molybdates and Tungstates of Mono- and Trivalent Elements as Possible Ferroelastics and Ferroelectrics. *Ferroelectrics* **2005**, *321*, 63−90.

(5) Troitskaia, I. B.; Gavrilova, T. A.; Gromilov, S. A.; Sheglov, D. V.; Atuchin, V. V.; Vemuri, R. S.; Ramana, C. V. Growth and Structural Properties of α-MoO_3 (010) Microplates with Atomically Flat Surface. *Mater. Sci. Eng., B* **2010**, *174*, 159−163.

(6) Ramana, C. V.; Atuchin, V. V.; Groult, H.; Julien, C. M. Electrochemical Properties of Sputter-Deposited MoO_3 Films in Lithium Microbatteries. *J. Vac. Sci. Technol., A* **2012**, *30*, 04D105.

(7) Sarapulova, A. E.; Bazarov, B.; Namsaraeva, T.; Dorzhieva, S.; Bazarova, J.; Grossman, V.; Bush, A. A.; Antonyshyn, I.; Schmidt, M.; Bell, A. M. T.; et al. Possible Piezoelectric Materials $CsMZr_{0.5}(MoO_4)_3$ (M = Al, Sc, V, Cr, Fe, Ga, In) and $CsCrTi_{0.5}(MoO_4)_3$: Structure and Physical Properties. *J. Phys. Chem. C* **2014**, *118*, 1763−1773.

(8) Atuchin, V. V.; Ivannikova, N. V.; Komonov, A. I.; Kuratieva, N. V.; Loshkarev, I. D.; Pervukhina, N. V.; Pokrovsky, L. D.; Shlegel, V. N. The Low Thermal Gradient Czochralski Crystal Growth and Microstructural Properties of a Pb_2MoO_5(20−1) Cleaved Surface. *CrystEngComm* **2015**, *17*, 4512−4516.

(9) Kaczmarek, A. M.; Van Deun, R. Rare Earth Tungstate and Molybdate Compouds − from 0D to 3D Architectures. *Chem. Soc. Rev.* **2013**, *42*, 8835−8848.

(10) Enterkin, J. A.; Maggard, P. A.; Ishiwata, S.; Marks, L. D.; Poeppelmeier, K. R.; Azuma, M.; Takano, M. Single Crystal Growth and Structure of $La_4Cu_3MoO_{12}$. *J. Solid State Chem.* **2010**, *183*, 551−556.

(11) Atuchin, V. V.; Chimitova, O. D.; Gavrilova, T. A.; Molokeev, M. S.; Kim, S.-J.; Surovtsev, N. V.; Bazarov, B. G. Synthesis, Structural and Vibrational Properties of Microcrystalline $RbNd(MoO_4)_2$. *J. Cryst. Growth* **2011**, *318*, 683−686.

(12) Atuchin, V. V.; Grossman, V. G.; Adichtchev, S. V.; Surovtsev, N. V.; Gavrilova, T. A.; Bazarov, B. G. Structural and Vibrational Properties of Microcrystalline $TlM(MoO_4)_2$ (M = Nd, Pr) Molybdates. *Opt. Mater.* **2012**, *34*, 812−816.

DOI: 10.1021/acs.jpcc.6b01489
J. Phys. Chem. C 2016, 120, 10559−10568

(13) Yu, Y.; Li, L. G.; Lin, Z. B.; Wang, G. F. Growth, Structure and Optical Properties of a Nonlinear Optical Crystal α-$LaBMoO_6$. *CrystEngComm* **2013**, *15*, 5245−5249.
(14) Atuchin, V. V.; Aleksandrovsky, A. S.; Chimitova, O. D.; Krylov, A. S.; Molokeev, M. S.; Bazarov, B. G.; Bazarova, J. G.; Xia, Z. G. Synthesis and Spectroscopic Properties of Multiferroic β'-$Tb_2(MoO_4)_3$. *Opt. Mater.* **2014**, *36*, 1631−1635.
(15) Lim, C. S.; Aleksandrovsky, A.; Molokeev, M.; Oreshonkov, A.; Atuchin, V. The Modulated Structure and Frequency Upconversion Properties of $CaLa_2(MoO_4)_4$:Ho^{3+}/Yb^{3+} Phosphors Prepared by Microwave Synthesis. *Phys. Chem. Chem. Phys.* **2015**, *17*, 19278−19287.
(16) Tanner, P. A. Some Misconceptions Concerning the Electronic Spectra of Tri-Positive Europium and Cerium. *Chem. Soc. Rev.* **2013**, *42*, 5090−5101.
(17) Parchur, A. K.; Prasad, A. I.; Rai, S. B.; Tewari, R.; Sahu, R. K.; Okram, G. S.; Singh, R. A.; Ningthoujam, R. S. Observation on Intermadiate Bands in Eu^{3+} doped YPO_4 Host: Li^+ Ion Effect and Blue to Pink Light Emitter. *AIP Adv.* **2012**, *2*, 032119.
(18) Ko, Y. H.; Lee, S. H.; Yu, J. S. Luminescence Properties of Europium Ions-Doped Yttrium Silicate (Y_2SiO_5:Eu^{3+}) Nanocrystalline Phosphors: Effects of Eu^{3+} Ion Concentration and Thermal Annealing. *J. Nanosci. Nanotechnol.* **2013**, *13*, 3230−3235.
(19) Shi, P. L.; Xia, Z. G.; Molokeev, M. S.; Atuchin, V. V. Crystal Chemistry and Luminescence Properties of Red-Emitting $CsGd_{1-x}Eu_x(MoO_4)_2$ Solid-Solution Phosphors. *Dalton Trans.* **2014**, *43*, 9669−9676.
(20) Morozov, V. A.; Lazoryak, B. I.; Shmurak, S. Z.; Kiselev, A. P.; Lebedev, O. I.; Gauquelin, N.; Verbeeck, J.; Hadermann, J.; Van Tendeloo, G. Influence of the Structure on the Properties of $Na_xEu_y(MoO_4)_z$ Red Phosphors. *Chem. Mater.* **2014**, *26*, 3238−3248.
(21) Ji, H. P.; Huang, Z. H.; Xia, Z. G.; Molokeev, M. S.; Jiang, X. X.; Lin, Z. H.; Atuchin, V. V. Comparative Investigations of the Crystal Structure and Photoluminescence Property of Eulytite-Type $Ba_3Eu(PO_4)_3$ and $Sr_3Eu(PO_4)_3$. *Dalton Trans.* **2015**, *44*, 7679−7686.
(22) Xia, Z. G.; Zhang, Y. Y.; Molokeev, M. S.; Atuchin, V. V. Structural and Luminescence Properties of Yellow-Emitting $NaScSi_2O_6$:Eu^{2+} Phosphors: Eu^{2+} Site Preference Analysis and Generation of Red Emission by Codoping Mn^{2+} for White-Light-Emitting Diode Applications. *J. Phys. Chem. C* **2013**, *117*, 20847−20854.
(23) Ji, H. P.; Huang, Z. H.; Xia, Z. G.; Molokeev, M. S.; Atuchin, V. V.; Fang, M. H.; Huang, S. F. New Yellow-Emitting Whitlockite-Type Structure $Sr_{1.75}Ca_{1.25}(PO_4)_2$:$Eu^{2+}$ Phosphor for Near-UV Pumped White Light-Emitting Devices. *Inorg. Chem.* **2014**, *53*, 5129−5135.
(24) Xia, Z. G.; Zhang, Y. Y.; Molokeev, M. S.; Atuchin, V. V.; Luo, Y. Linear Structural Evolution Induced Tunable Photoluminescence in Clinopyroxene Solid-Solution Phosphors. *Sci. Rep.* **2013**, *3*, 3310.
(25) Boulahya, K.; Parras, M.; González-Calbet, J. M. Synthesis, Structural and Magnetic Characterization of a New Scheelite Related Compound: $Eu_2Mo_3O_{12}$. *Eur. J. Inorg. Chem.* **2005**, *5*, 967−970.
(26) Atuchin, V. V.; Aleksandrovsky, A. S.; Chimitova, O. D.; Gavrilova, T. A.; Krylov, A. S.; Molokeev, M. S.; Oreshonkov, A. S.; Bazarov, B. G.; Bazarova, J. G. Synthesis and Spectroscopic Properties of Monoclinic a-$Eu_2(MoO_4)_3$. *J. Phys. Chem. C* **2014**, *118*, 15404−15411.
(27) Guzmán-Afonso, C.; León-Luis, S. F.; Sans, J. A.; González-Silgo, C.; Rodríguez-Hernández, P.; Radescu, S.; Muñoz, A.; López-Solano, J.; Errandonea, D.; Manjón, F. J.; et al. Experimental and Theoretical Study of α-$Eu_2(MoO_4)_3$ under Compression. *J. Phys.: Condens. Matter* **2015**, *27*, 465401.
(28) Atuchin, V. V.; Bazarov, B. G.; Gavrilova, T. A.; Grossman, V. G.; Molokeev, M. S.; Bazarova, Zh. G. Preparation and Structural Properties of Nonlinear Optical Borates $K_{2(1-x)}Rb_{2x}Al_2B_2O_7$, $0 < x < 0.75$. *J. Alloys Compd.* **2012**, *515*, 119−122.
(29) Golovnev, N.; Molokeev, M. Bridging Behavior of the 2-thiobarbiturate Anion in its Complexes with Li-I and Na-I. *Acta Crystallogr., Sect. C: Cryst. Struct. Commun.* **2013**, *69*, 704−708.
(30) *Bruker AXS TOPAS V4: General profile and structure analysis software for powder diffraction data. − User's Manual*. Bruker AXS: Karlsruhe, Germany. 2008.
(31) Moss, T. S. *Optical Properties of Semiconductors*; Butterworth: London, 1961.
(32) Atuchin, V. V.; Isaenko, L. I.; Kesler, V. G.; Kang, L.; Lin, Z. S.; Molokeev, M. S.; Yelisseyev, A. P.; Zhurkov, S. A. Structural, Spectroscopic, and Electronic Properties of Cubic G0-Rb_2KTiOF_5 Oxyfluoride. *J. Phys. Chem. C* **2013**, *117*, 7269−7278.
(33) Errandonea, D.; Muñoz, A.; Rodríguez-Hernandez, P.; Proctor, J. E.; Sapiña, F.; Bettinelli, M. Theoretical and Experimental Study of the Crystal Structures, Lattice Vibrations, and Band Structures of Monazite-Type $PbCrO_4$, $PbSeO_4$, $SrCrO_4$, and $SrSeO_4$. *Inorg. Chem.* **2015**, *54*, 7524−7535.
(34) Ivanov, D. V.; Pinaeva, L. G.; Isupova, L. A.; Sadovskaya, E. M.; Prosvirin, I. P.; Gerasimov, E. Y.; Yakovleva, I. S. Effect of Surface Decoration with $LaSrFeO_4$ on Oxygen Mobility and Catalytic Activity of $La_{0.4}Sr_{0.6}FeO_{3-\delta}$ in High-Temperature N_2O Decomposition, Methane Combustion and Ammonia Oxidation. *Appl. Catal., A* **2013**, *457*, 42−51.
(35) Taran, O. P.; Ayusheev, A. B.; Ogorodnikova, O. L.; Prosvirin, I. P.; Isupova, L. A.; Parmon, V. N. Perovskite-Like Catalysts $LaBO_3$ (B = Cu, Fe, Mn, Co, Ni) for Wet Peroxide Oxidation of Phenol. *Appl. Catal., B* **2016**, *180*, 86−93.
(36) Scofield, J. H. Hartree-Slater Subshell Photoionization Cross-Sections at 1254 and 1487 eV. *J. Electron Spectrosc. Relat. Phenom.* **1976**, *8*, 129−137.
(37) Rubio, E. J.; Atuchin, V. V.; Kruchinin, V. N.; Pokrovsky, L. D.; Prosvirin, I. P.; Ramana, C. V. Electronic Structure and Optical Quality of Nanocrystalline Y_2O_3 Film Surfaces and Interfaces on Silicon. *J. Phys. Chem. C* **2014**, *118*, 13644−13651.
(38) Blaha, P.; Schwarz, K.; Madsen, G.; Kvasnicka, D.; Luitz, J. *WIEN2k, An Augmented Plane Wave plus Local Orbitals Program for Calculating Crystal Properties*; Vienna University of Technology: Austria,(2001).
(39) Perdew, J. P.; Burke, K.; Ernzerhof, M. Generalized Gradient Approximation Made Simple. *Phys. Rev. Lett.* **1996**, *77*, 3865−3868.
(40) Anisimov, V. I.; Solovyev, I. V.; Korotin, M. A.; Czyzyk, M. T.; Sawatzky, G. A. Density-Functional Theory and NiO Photoemission Spectra. *Phys. Rev. B: Condens. Matter Mater. Phys.* **1993**, *48*, 16929−16934.
(41) Liechtenstein, A. I.; Anisimov, V. I.; Zaanen, J. Density-Functional Theory and Strong Interactions: Orbital Ordering in Mott-Hubbard Insulators. *Phys. Rev. B: Condens. Matter Mater. Phys.* **1995**, *52*, R5467−R5470.
(42) Andersen, O. K. Linear Methods in Band Theory. *Phys. Rev. B* **1975**, *12*, 3060−3083.
(43) Perdew, J. P.; Wang, Y. Accurate and Simple Analytic Representation of the Electron-Gas Correlation Energy. *Phys. Rev. B: Condens. Matter Mater. Phys.* **1992**, *45*, 13244−13249.
(44) Ibrahim, I. A. M.; Lenčéš, Z.; Šajgalík, P.; Benco, L. Electronic Structure and Energy Level Schemes of RE^{3+}:$LaSi_3N_5$ and RE^{2+}:$LaSi_3N_{5-x}O_x$ Phosphors (RE = Ce, Pr, Nd, Pm, Sm, Eu) from first principles. *J. Lumin.* **2015**, *164*, 131−137.
(45) Ibrahim, I. A. M.; Lenčéš, Z.; Benco, L.; Šajgalík, P. Lanthanide-Doped $LaSi_3N_5$ Based Phosphors: *Ab initio* Study of Electronic Structures, Bandgaps, and Energy Level Locations. *J. Lumin.* **2016**, *172*, 83−91.
(46) Bazarov, B. G.; Chimitova, O. D.; Klevtsova, R. F.; Tushinova, Y. L.; Glinskaya, L. A.; Bazarova, Z. G. Crystal Structure of a New Ternary Molybdate in the Rb_2MoO_4-$Eu_2(MoO_4)_3$-$Hf(MoO_4)_2$ System. *J. Struct. Chem.* **2008**, *49*, 53−57.
(47) Chimitova, O. D.; Atuchin, V. V.; Bazarov, B. G.; Molokeev, M. S.; Bazarova, Z. G. The Formation and Structural Parameters of New Double Molybdates $RbLn(MoO_4)_2$ (Ln = Pr, Nd, Sm, Eu). *Proc. SPIE* **2013**, *8771*, 87711A.
(48) Marinova, V.; Veleva, M. Refractive Index Measurements and Transmission Spectra of $Bi_2(MoO_4)_3$ Single Crystals. *Opt. Mater.* **2002**, *19*, 329−333.

DOI: 10.1021/acs.jpcc.6b01489
J. Phys. Chem. C 2016, 120, 10559−10568

(49) Coquin, G. A.; Pinnow, D. A.; Warner, A. W. Physical Properties of Lead Molybdate Relevant to Acousto-Optic Device Applications. *J. Appl. Phys.* **1971**, *42*, 2162−2168.
(50) Chernyak, D. M.; Danevich, F. A.; Degoda, V.; Ya; Giuliani, A.; Ivanov, I. M.; Kogut, Ya. P.; Kraus, H.; Kropivyansky, B. N.; Makarov, E. P.; Mancuso, M.; et al. Effect of Tungsten Doping on $ZnMoO_4$ Scintillating Bolometer Performance. *Opt. Mater.* **2015**, *49*, 67−74.
(51) Ivleva, L. I.; Voronina, I. S.; Berezovskaya, L.; Yu; Lykov, P. A.; Osiko, V. V.; Iskhakova, L. D. Growth and Properties of $ZnMoO_4$ Single Crystals. *Crystallogr. Rep.* **2008**, *53*, 1087−1090.
(52) Van Deun, R.; Binnemans, K.; Goller-Walrand, C.; Adam, J. L. Optical Properties of Eu^{3+}-Doped Fluorophospate Glasses. *J. Phys.: Condens. Matter* **1998**, *10*, 7231−7241.
(53) Binnemans, K.; Gorller-Walrand, C. Optical Absorption Spectra of Eu^{3+} in $Y_3Ga_5O_{12}$ (YGG). *J. Phys.: Condens. Matter* **1997**, *9*, 1637−1648.
(54) Sviridov, D. G.; Sviridova, R. K.; Smirnov, Yu. F. *Optical Spectra of Transition Metal Ions in Crystals*; Nauka: Moscow, 1976 (in Russian).
(55) Kwolek, P.; Tokarski, T.; Lokcik, T.; Szacilowski, K. Novel, Microvave Assisted Route of Synthesis of Binary Oxide Semiconducting Phases - $PbMoO_4$ and $PbWO_4$. *Arch. Metall. Mater.* **2013**, *58*, 217−222.
(56) Sczancoski, J. C.; Cavalcante, L. S.; Joya, M. R.; Varela, J. A.; Pizani, P. S.; Longo, E. $SrMoO_4$ Powders Processed in Microwave-Hydrothermal: Synthesis, Sharacterization and Optical Properties. *Chem. Eng. J.* **2008**, *140*, 632−637.
(57) Spassky, D. A.; Vasil'ev, A. N.; Kamenskikh, I. A.; Mikhailin, V. V.; Savon, A. E.; Hizhnyi, Yu. A.; Nedilko, S. G.; Lykov, P. A. Electronic Structure and Luminescence Mechanisms in $ZnMoO_4$ Crystals. *J. Phys.: Condens. Matter* **2011**, *23*, 365501.
(58) Ramana, C. V.; Atuchin, V. V.; Kesler, V. G.; Kochubey, V. A.; Pokrovsky, L. D.; Shutthanandan, V.; Becker, U.; Ewing, R. C. Growth and Surface Characterization of Sputter-Deposited Molybdenum Oxide Thin Films. *Appl. Surf. Sci.* **2007**, *253*, 5368−5374.
(59) Zhang, Z. Y.; Hu, C. G.; Hashim, M.; Chen, P.; Xiong, Y. Q.; Zhang, C. L. Synthesis and Magnetic Property of $FeMoO_4$ Nanorods. *Mater. Sci. Eng., B* **2011**, *176*, 756−761.
(60) Im, H.-N.; Choi, M.-B.; Jeon, S.-Y.; Song, S.-J. Structure, Thermal Stability and Electrical Conductivity of $CaMoO_{4+\delta}$. *Ceram. Int.* **2011**, *37*, 49−53.
(61) Atuchin, V. V.; Molokeev, M. S.; Yurkin, G.; Yu; Gavrilova, T. A.; Kesler, V. G.; Laptash, N. M.; Flerov, I. N.; Patrin, G. S. Synthesis, Structural, Magnetic, and Electronic Properties of Cubic $CsMnMoO_3F_3$ Oxyfluoride. *J. Phys. Chem. C* **2012**, *116*, 10162−10170.
(62) Atuchin, V. V.; Khyzhun, O. Y.; Chimitova, O. D.; Molokeev, M. S.; Gavrilova, T. A.; Bazarov, B. G.; Bazarova, J. G. Electronic Structure of β-$RbNd(MoO_4)_2$ by XPS and XES. *J. Phys. Chem. Solids* **2015**, *77*, 101−108.
(63) Atuchin, V. V.; Aleksandrovsky, A. S.; Chimitova, O. D.; Diao, C.-P.; Gavrilova, T. A.; Kesler, V. G.; Molokeev, M. S.; Krylov, A. S.; Bazarov, B. G.; Bazarova, J. G.; et al. Electronic Structure of b-$RbSm(MoO_4)_2$ and Chemical Bonding in Molybdates. *Dalton Trans.* **2015**, *44*, 1805−1815.
(64) Teterin, Yu. A.; Bondarenko, T. N.; Teterin, A. Yu; Lebedev, A. M.; Utkin, I. O. XPS of Lanthanoide Orthoniobates. *J. Electron Spectrosc. Relat. Phenom.* **1998**, *96*, 221−228.
(65) Cho, E.-J.; Oh, S.-J. Surface Valence Transition in Trivalent Eu Insulating Compounds Observed by Photoelectron Spectroscopy. *Phys. Rev. B: Condens. Matter Mater. Phys.* **1999**, *59*, R15613−R15616.
(66) Teterin, Yu. A.; Teterin, A. Yu. Structure of X-ray Photoelectron Spectra of Lanthanide Compounds. *Russ. Chem. Rev.* **2002**, *71*, 347−381.
(67) Mercier, F.; Alliot, C.; Bion, L.; Thromat, N.; Toulhoat, P. XPS Study of Eu(III) Coordination Compounds: Core Levels Binding Energies in Solid Mixed-Oxo-Compounds $Eu_mX_xO_y$. *J. Electron Spectrosc. Relat. Phenom.* **2006**, *150*, 21−26.
(68) Chae, K.-W.; Park, T.-R.; Cheon, C. I.; Cho, N. I.; Kim, J. S. The Enhancement of Luminescence in Co-Doped Cubic Eu_2O_3 Using Li^+ and Al^{3+} Ions. *J. Lumin.* **2011**, *131*, 2597−2605.
(69) Kang, J.-G.; Jung, Y. K.; Min, B.-K.; Sohn, Y. K. Full Characterization of $Eu(OH)_3$ and Eu_2O_3 Nanorods. *Appl. Surf. Sci.* **2014**, *314*, 158−165.
(70) Khyzhun, O. Yu. XPS, XES and XAS Studies of the Electronic Structure of Tungsten Oxides. *J. Alloys Compd.* **2000**, *305*, 1−6.
(71) Atuchin, V. V.; Kesler, V. G.; Maklakova, N. Yu.; Pokrovsky, L. D. Core Level Spectroscopy and RHEED Analysis of $KGd(WO_4)_2$ Surface. *Solid State Commun.* **2005**, *133*, 347−351.
(72) Atuchin, V. V.; Pokrovsky, L. D.; Khyzhun, O. Yu; Sinelnichenko, A. K.; Ramana, C. V. Surface Crystallography and Electronic Structure of Potassium Yttrium Tungstate. *J. Appl. Phys.* **2008**, *104*, 033518.
(73) Atuchin, V. V.; Galashov, E. N.; Khyzhun, O. Yu; Kozhukhov, A. S.; Pokrovsky, L. D.; Shlegel, V. N. Structural and Electronic Properties of $ZnWO_4$(010) Cleaved Surface. *Cryst. Growth Des.* **2011**, *11*, 2479−2484.
(74) Atuchin, V. V.; Galashov, E. N.; Khyzhun, O. Y.; Bekenev, V. L.; Pokrovsky, L. D.; Borovlev, Yu. A.; Zhdankov, V. N. Low Thermal Gradient Czochralski Growth of Large $CdWO_4$ Crystals and Electronic Properties of (010) Cleaved Surface. *J. Solid State Chem.* **2016**, *236*, 24−31.
(75) Khyzhun, O. Yu.; Strunskus, T.; Solonin, Yu. M. XES, XPS and NEXAFS Studies of the Electronic Structure of Cubic $MoO_{1.9}$ and $H_{1.63}MoO_3$ Thick Films. *J. Alloys Compd.* **2004**, *366*, 54−60.
(76) Chaika, A. N.; Ionov, A. M.; Maslov, K. A.; Mukovskii, Ya. M. Electron Spectroscopy of the $Ln_{1-x}Sr_xMnO_3$ (Ln = La, Ce, Pr, Eu) Compounds. *Phys. Low-Dim. Struct.* **2001**, *11/12*, 201−210.
(77) Zhu, W.; Zhang, Y.-J.; He, H.-M.; Fang, Z.-Y. Synthesis and Luminescence Property of Hierarchical Europium Oxalate Microparticles. *Chin. J. Chem. Phys.* **2011**, *24*, 65−69.
(78) Li, J.-M.; Zeng, X.-L.; Dong, Y.-H.; Xu, Z.-A. White-Light Emission and Weak Antiferromagnetism from Cubic Rare-Earth Oxide Eu_2O_3 Electrospun Nanostructures. *CrystEngComm* **2013**, *15*, 2372−2377.
(79) Petrov, D.; Angelov, B.; Lovchinov, V. Magnetic Susceptibility and Surface Properties of $EuAlO_3$ Nanocrystals. *J. Alloys Compd.* **2011**, *509*, 5038−5041.
(80) Atuchin, V. V.; Kesler, V. G.; Pervukhina, N. V.; Zhang, Z. M. Ti 2p and O 1s Core Levels and Chemical Bonding in Titanium-Bearing Oxides. *J. Electron Spectrosc. Relat. Phenom.* **2006**, *152*, 18−24.
(81) Atuchin, V. V.; Kesler, V. G.; Pervukhina, N. V. Electronic and Structural Parameters of Phosphorus-Oxygen Bonds in Inorganic Phosphate Crystal. *Surf. Rev. Lett.* **2008**, *15*, 391−399.
(82) Atuchin, V. V.; Isaenko, L. I.; Kesler, V. G.; Kang, L.; Lin, Z. S.; Molokeev, M. S.; Yelisseyev, A. P.; Zhurkov, S. A. Structural, Spectroscopic, and Electronic Properties of Cubic G0-Rb_2KTiOF_5 Oxyfluoride. *J. Phys. Chem. C* **2013**, *117*, 7269−7278.
(83) Atuchin, V. V.; Kaichev, V. V.; Korolkov, I. V.; Saraev, A. A.; Troitskaia, I. B.; Perevalov, T. V.; Gritsenko, V. A. Electronic Structure of Noncentrosymmentric α-GeO_2 with Oxygen Vacancy: *ab initio* Calculations and Comparison with Experiment. *J. Phys. Chem. C* **2014**, *118*, 3644−3650.
(84) Atuchin, V. V.; Kalabin, I. E.; Kesler, V. G.; Pervukhina, N. V. Nb 3d and O 1s Core Levels and Chemical Bonding in Niobates. *J. Electron Spectrosc. Relat. Phenom.* **2005**, *142*, 129−134.
(85) López-Moreno, S.; Rodríguez-Hernández, P.; Muñoz, A.; Romero, A. H.; Errandonea, D. First-Principles Calculations of Electronic, Vibrational, and Structural Properties of Scheelite $EuWO_4$ under Pressure. *Phys. Rev. B: Condens. Matter Mater. Phys.* **2011**, *84*, 064108.
(86) Liu, X.; Li, L.; Noh, H. M.; Moon, B. K.; Choi, B. C.; Jeong, J. H. Chemical Bond Properties and Charge Transfer Bands of O^{2-}−Eu^{3+}, O^{2-} − Mo^{6+} and O^{2-}−W^{6+} in Eu^{3+}-Doped Garnet Hosts $Ln_3M_5O_{12}$ and ABO_4 Molybdate and Tungstate Phosphors. *Dalton Trans.* **2014**, *43*, 8814−8825.

DOI: 10.1021/acs.jpcc.6b01489
J. Phys. Chem. C 2016, 120, 10559−10568